Journal of Sound and Vibration (1997) **208**(3), 457–474

DYNAMIC ANALYSIS OF A ROTOR SYSTEM CONSIDERING A SLANT CRACK IN THE SHAFT

A. S. Sekhar and P. Balaji Prasad

Department of Mechanical Engineering, Indian Institute of Technology, Kharagpur—721 302, India

(*Received* 10 *March* 1997, *and in final form* 8 *July* 1997)

The dynamic behaviour of structures—in particular, rotors containing cracks—is a subject of considerable current interest. Several researchers have developed models of cracked rotor systems considering mainly the transverse surface crack. In the present study finite element (FEM) analysis of a rotor–bearing system for flexural vibrations has been considered by including a shaft having a slant crack that has resulted from the fatigue of the shaft due to the torsional moment. A flexibility matrix for a slant crack and later the stiffness matrix of a slant cracked element have been developed to be used subsequently in the FEM analysis of the rotor–bearing system. The frequency spectrum of the steady state response of the cracked rotor was found to have sub-harmonic frequency components at an interval frequency corresponding to the torsional frequency, which can be used for crack detection.

1. INTRODUCTION

One form of damage that can lead to catastrophic failure if undetected is fatigue cracks in the shaft. Several researchers have developed models of cracked rotor systems in order to predict the change in vibrational behaviour due to crack growth.

The first studies on cracked rotors were started in the 1970s by Dimarogonas [1] and Pafelias [2], although the fact that a crack affects the dynamic response of a structural member was known long ago through the attempts of Kirmser [3] and Thomson [4]. Since then, many researchers have realized the importance of the cracked structures; in particular, the dynamics of cracked rotors, which is well documented in a book by Dimarogonas and Paipetis [5], followed by a literature survey by Wauer [6] and, more recently, a survey on simple rotors by Gasch [7] and a review on general cracked structures by Dimarogonas [8].

However, all of the works reported in [5–8] consider mainly the transverse crack of the shaft, which occurs as a result of fatigue of shaft material due to an excessive bending moment. Ichimonji and Watanabe [9] considered a slant crack that occurs from the fatigue of the shaft due to the torsional moment, and studied the dynamics of a simple rotor for qualitative analysis. Extending this work [9], Ichimonji *et al*. [10] presented, using 3-D FEM, a quantitative analysis of a rotor with a slant crack. To the best of the authors' knowledge, references [9, 10] are the only works on a slant crack. Hence, attention to the study of rotor system with slant cracks is required, as the use of large rotating machines driven under operating systems which are apt to induce torsional vibration, such as daily start and stop operation or thyristor motor driving, has increased recently.

0022–460X/97/480457 + 18 $25.00/0/sv971222

In the present study, FEM analysis of a rotor–bearing system for flexural vibrations has been considered by including a shaft having a slant crack. The present study involves deriving a flexibility matrix for the slant crack, on similar lines as the work of Papadopoulos and Dimarogonas [11] for a transverse crack. This will be used to develop a stiffness matrix of a cracked element, to be used subsequently in the FEM analysis of the rotor–bearing system.

2. THEORY

As discussed in reference [9], the development of a slant crack can be understood by considering the shaft element shown in Figure 1(a). Applying a torsional moment, M_Z to shaft causes primary stresses on its surface, and they are orthogonal to each other at an angle of 45° towards the axis of the shaft. When a torsional vibratory moment is applied to the shaft under the condition of a smaller amplitude over a longer period, a slant crack can grow along the primary stress line [9], as shown in Figure 1(b). The positive torsional moment puts tensional stress on the surfaces of the crack in such a way as to open it. On the other hand, negative torsional moment applies compressional stress, causing the crack to close.

The change in stiffness according to the "breathing" (crack open and close) of the crack is explained in detail in section 4. The slant crack may develop in three modes, and the cross-sections of the rotor with these three different types of slant crack are shown in Figure 2. In the present study, a quarter crack is considered for the analysis.

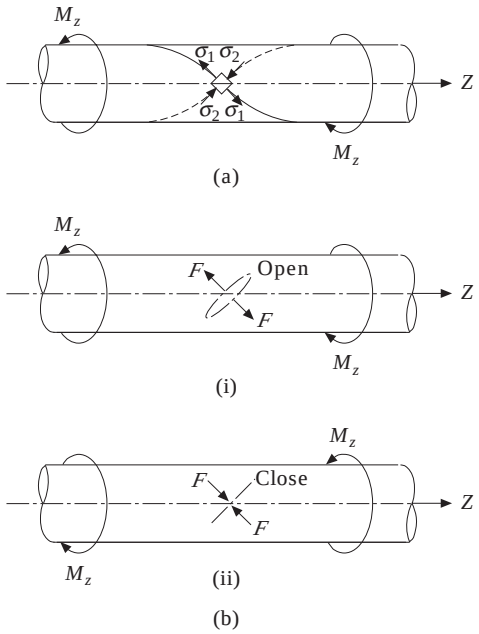

Figure 1. (a). The primary stress directions of a shaft under torsional loading (from reference [9]). (b) The breathing behaviour of a slant crack (from reference [9]): (i) $M_Z > 0$; (ii) $M_Z < 0$.

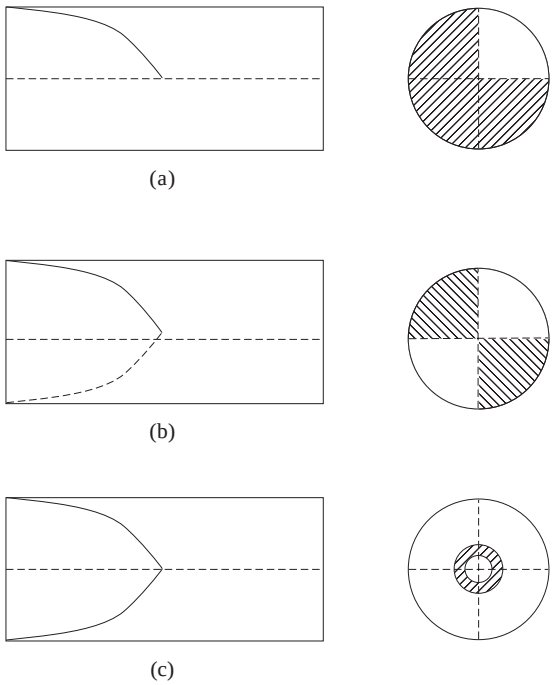

Figure 2. The slant crack configuration (from reference [10]). (a) Quarter crack; (b) half crack; (c) round crack.

3. CRACK MODELLING

3.1. FLEXIBILITY MATRIX OF CRACKED SECTION

Consider a rotor–bearing system with a slant crack as shown in Figure 3. The rotor is discretized into finite beam elements. Each element has two nodes with six degrees of freedom (d.o.f.) at each node. The shaft element is loaded with axial force P1, shear forces P2 and P3, bending moments P4 and P5 and torsional moment P6, and these result in a nodal vector $\{q\}$, as shown by q_1–q_{12} in Figure 3.

The details of a cracked cross-section with slant crack of depth α along the minor axis of the slant section are given in Figure 4. The section along the crack direction which will be at 45° degrees to the shaft axis is an ellipse of major axis $D/\cos 45^\circ$ and minor axis D.

Proceeding in a similar away as in reference [11] for a transverse crack, the compliance matrix for a slant cracked section has been developed in the present study.

The Paris equation gives the additional displacement u_i due to a crack depth of α in the ith direction as

$$u_i = \frac{\partial}{\partial p_i} \int_0^{\alpha} J(\alpha)\, \mathrm{d}\alpha, \tag{1}$$

where $J(\alpha)$ is the strain energy density function (SEDF) and p_i is the corresponding load. The SEDF is

$$J(\alpha) = \frac{1}{E'} \left[\left(\sum_{i=1}^{6} K_{Ii} \right)^2 + \left(\sum_{i=1}^{6} K_{IIi} \right)^2 + m \left(\sum_{i=1}^{6} K_{IIIi} \right)^2 \right]. \tag{2}$$

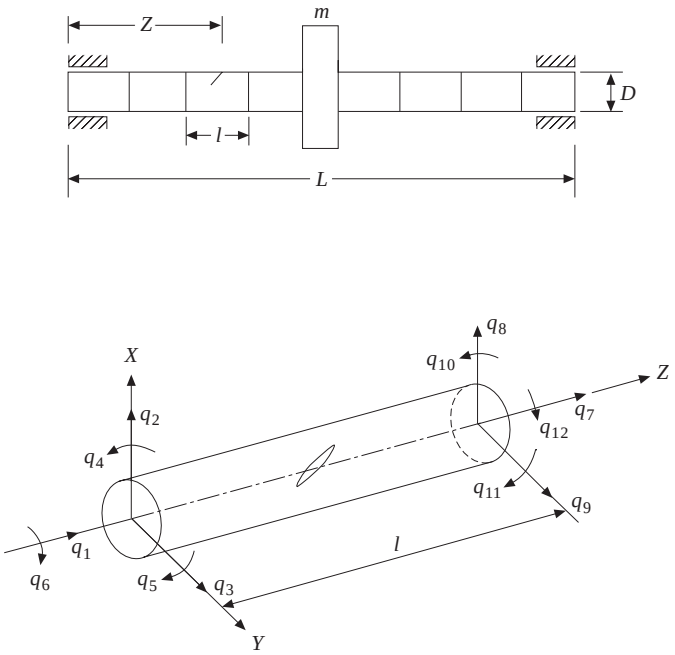

Figure 3. A rotor–bearing system model with a slant crack element.

where $E' = E$ or $E/(1 - v^2)$ for plane stress and plane strain conditions respectively and $m = 1 + v$. The K_{ij} are the stress intensity factors (SIF) for $i = \text{I, II and III}$ modes; namely, the opening type, sliding type and tearing type cracks, for $1, 2, \ldots, 6$ load index. A list of nomenclature is given in the Appendix.

The local flexibility due to the crack per unit width is given by the definition

$$c_{ij} = \frac{\partial u_i}{\partial p_j} = \frac{\partial}{\partial p_i}\left[\frac{\partial}{\partial p_j}\int_0^{\alpha} J(\alpha)\,\mathrm{d}\alpha\right] \tag{3}$$

After integration along the width b (along the semi-major axis for the quarter crack) of the crack of depth α (along the semi-minor axis),

$$c_{ij} = \frac{\partial^2}{\partial p_i\,\partial p_j}\int_0^{b}\int_0^{\alpha} J(\alpha)\,\mathrm{d}\alpha\,\mathrm{d}x. \tag{4}$$

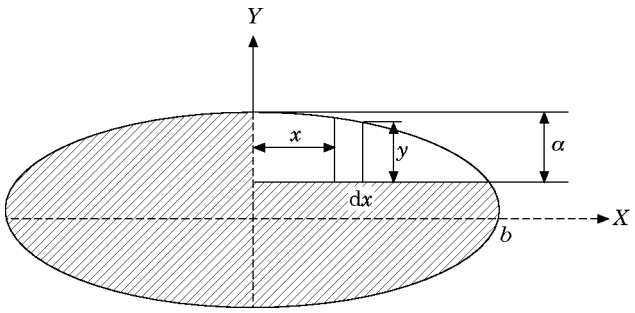

Figure 4. The details of the slant crack section.

The values of SIF in equation (2) for a strip of unit thickness with a slant crack are calculated as

$$K_{I1} = \sigma_1\sqrt{\pi\alpha}\, F_1(\alpha/h), \qquad \sigma_1 = \frac{P_1}{\sqrt{2}\pi R^2},$$

$$K_{I4} = \sigma_4\sqrt{\pi\alpha}\, F_1(\alpha/h), \qquad \sigma_4 = \frac{\sqrt{2}P_4 x}{\pi R^4},$$

$$K_{I5} = \sigma_5\sqrt{\pi\alpha}\, F_2(\alpha/h), \qquad \sigma_5 = \frac{2P_5}{\pi R^4}(2R^2 - x^2)^{1/2},$$

$$K_{I2} = K_{I3} = K_{I6} = 0,$$

$$K_{II3} = \sigma_3\sqrt{\pi\alpha}\, F_{II}(\alpha/h), \qquad \sigma_3 = \frac{kP_3}{\sqrt{2}\pi R^2}$$

$$K_{II6} = \sigma_{6II}\sqrt{\pi\alpha}\, F_{II}(\alpha/h), \qquad \sigma_{6II} = \frac{P_6 x}{\sqrt{2}\pi R^4}(2R^2 - x^2)^{1/2},$$

$$K_{II1} = K_{II2} = K_{II4} = K_{II5} = 0,$$

$$K_{III2} = \sigma_2\sqrt{\pi\alpha}\, F_{III}(\alpha/h), \qquad \sigma_2 = \frac{kP_2}{\sqrt{2}\pi R^2},$$

$$K_{III6} = \sigma_{6III}\sqrt{\pi\alpha}\, F_{III}(\alpha/h), \qquad \sigma_{6III} = \frac{P_6 x}{\pi R^4}(2R^2 - x^2)^{1/2},$$

$$K_{III1} = K_{III3} = K_{III4} = K_{III5} = 0, \tag{5}$$

where

$$F_1(\alpha/h) = \frac{(\tan\lambda)^{1/2}}{\lambda^{1/2}}[0{\cdot}752 + 2{\cdot}02(\alpha/h) + 0{\cdot}37(1 - \sin\lambda)^3]/\cos\lambda,$$

$$F_2(\alpha/h) = \frac{(\tan\lambda)^{1/2}}{\lambda^{1/2}}[0{\cdot}923 + 0{\cdot}199(1 - \sin\lambda)^4]/\cos\lambda,$$

$$F_{II}(\alpha/h) = [1{\cdot}122 - 0{\cdot}561(\alpha/h) + 0{\cdot}085(\alpha/h)^2 + 0{\cdot}18(\alpha/h)^3](1 - \alpha/h)^{1/2},$$

$$F_{III}(\alpha/h) = (\tan\lambda)^{1/2}/\lambda^{1/2},$$

in which $\lambda = \pi\alpha/2h$, $h = (4R^2 - 2x^2)^{1/2}$ and $k = 6(1 + \nu)/(7 + 6\nu)$, assuming the same shape coefficient for the elliptic section.

From equations (1)–(4), we can derive the coefficients of the compliance matrix in non-dimensional form. These are given as follows:

$$\bar{c}_{11} = \pi ERc_{11}/(1-\nu^2) = \sqrt{2}\int_0^{\bar{a}}\int_0^{\bar{b}} \bar{y}F_1(\overline{h})^2\,\mathrm{d}\bar{x}\,\mathrm{d}\bar{y},$$

$$\bar{c}_{15} = \pi ER^2c_{15}/(1-\nu^2) = 4\sqrt{2}\int_0^{\bar{a}}\int_0^{\bar{b}} \bar{y}\sqrt{1-\bar{x}^2}\,F_1(\overline{h})F_2(\overline{h})\,\mathrm{d}\bar{x}\,\mathrm{d}\bar{y},$$

$$\bar{c}_{55} = \pi ER^3c_{55}/(1-\nu^2) = 16\sqrt{2}\int_0^{\bar{a}}\int_0^{\bar{b}} \bar{y}(1-\bar{x}^2)F_2^2(\overline{h})\,\mathrm{d}\bar{x}\,\mathrm{d}\bar{y},$$

$$\bar{c}_{44} = \pi ER^3c_{44}/(1-\nu^2) = 8\sqrt{2}\int_0^{\bar{a}}\int_0^{\bar{b}} \bar{y}\bar{x}^2F_1^2(\overline{h})\,\mathrm{d}\bar{x}\,\mathrm{d}\bar{y},$$

$$\bar{c}_{14} = \pi ER^2c_{14}/(1-\nu^2) = 4\int_0^{\bar{a}}\int_0^{\bar{b}} \bar{y}\bar{x}F_1^2(\overline{h})\,\mathrm{d}\bar{x}\,\mathrm{d}\bar{y},$$

$$\bar{c}_{45} = \pi ER^3c_{45}/(1-\nu^2) = 8\sqrt{2}\int_0^{\bar{a}}\int_0^{\bar{b}} \bar{y}\bar{x}\sqrt{1-\bar{x}^2}\,F_1(\overline{h})F_2(\overline{h})\,\mathrm{d}\bar{x}\,\mathrm{d}\bar{y},$$

$$\bar{c}_{33} = \pi ERc_{33}/(1-\nu^2) = \sqrt{2}\int_0^{\bar{a}}\int_0^{\bar{b}} \bar{y}F_{II}^2(\overline{h})\,\mathrm{d}\bar{x}\,\mathrm{d}\bar{y},$$

$$\bar{c}_{22} = \pi ERc_{22}/(1-\nu^2) = \sqrt{2}\int_0^{\bar{a}}\int_0^{\bar{b}} \bar{y}F_{III}^2(\overline{h})\,\mathrm{d}\bar{x}\,\mathrm{d}\bar{y},$$

$$\bar{c}_{62} = \pi ER^2c_{62}/(1-\nu^2) = 2\sqrt{2}\int_0^{\bar{a}}\int_0^{\bar{b}} \bar{y}\sqrt{(1-\bar{x}^2)}\,F_{III}^2(\overline{h})\,\mathrm{d}\bar{x}\,\mathrm{d}\bar{y},$$

$$\bar{c}_{63} = \pi ER^2c_{63}/(1-\nu^2) = 2\int_0^{\bar{a}}\int_0^{\bar{b}} \bar{y}\bar{x}F_{II}^2(\overline{h})\,\mathrm{d}\bar{x}\,\mathrm{d}\bar{y},$$

$$\bar{c}_{66} = \pi ER^3c_{66}/(1-\nu^2) = 8\int_0^{\bar{a}}\int_0^{\bar{b}} (A_1 + mA_2)\,\mathrm{d}\bar{x}\,\mathrm{d}\bar{y}, \tag{6}$$

where $\bar{y} = y/R$, $\bar{x} = x/\sqrt{2}R$, $\overline{h} = y/h$, $\bar{a} = \alpha/R$, $\overline{b} = b/\sqrt{2}R$, $A_1 = 0{\cdot}25\ \bar{x}^2\bar{y}F_{II}^2(\overline{h})\sqrt{2}$ and $A_2 = 0{\cdot}5(1-\bar{x}^2)\bar{y}F_{III}^2(\overline{h})\sqrt{2}$.

The local flexibility due to the crack can thus be written as a matrix, C_c, as

$$C_c = \frac{1}{F_0}\begin{bmatrix} \bar{c}_{11}R & & & & & \\ 0 & \bar{c}_{22}R & & & & \\ 0 & 0 & \bar{c}_{33}R & & \text{symmetric} & \\ \bar{c}_{41} & 0 & 0 & \bar{c}_{44}/R & & \\ \bar{c}_{51} & 0 & 0 & \bar{c}_{54}/R & \bar{c}_{55}/R & \\ 0 & \bar{c}_{62} & \bar{c}_{63} & 0 & 0 & \bar{c}_{66}/R \end{bmatrix},$$

where $F_0 = \pi ER^2/(1 - v^2)$, $R = D/2$ and $v = 0{\cdot}3$.

3.2. ELEMENT STIFFNESS MATRIX

Neglecting the shearing action and by using the strain energy, the flexibility coefficients for a section of an element without a crack can be derived in the form

$$C_0 = \begin{bmatrix} \dfrac{l}{AE} & & & & & \\ 0 & \dfrac{l^3}{3EI} & & & \text{symmetrical} & \\ 0 & 0 & \dfrac{l^3}{3EI} & & & \\ 0 & 0 & -\dfrac{l^2}{2EI} & \dfrac{l}{EI} & & \\ 0 & \dfrac{l^2}{2EI} & 0 & 0 & \dfrac{l}{EI} & \\ 0 & 0 & 0 & 0 & 0 & \dfrac{l}{GI_p} \end{bmatrix}.$$

A crack on a beam element introduces considerable local flexibility due to strain energy concentration in the vicinity of the crack tip under load. According to the Saint-Venant principle, the stress field is affected only in the region adjacent to the crack. The element stiffness matrix, except for the cracked element, may be regarded as unchanged under a certain limitation of element size [12]. It is very difficult to find an appropriate shape function to express the kinetic energy and elastic potential energy approximately, because of the discontinuity of deformation in the cracked element. However, the additional stress energy of a crack has been studied thoroughly in fracture mechanics and the flexibility coefficient, expressed by a stress intensity factor, can be easily derived, as discussed earlier in section 3.1. The shaft can be divided into finite elements (see Figure 3). The behaviour of the elements situated to the right of the cracked element may be regarded as external forces applied to the cracked element, while the behaviour of elements situated to its left may be regarded as constraints [12]. Thus the flexibility matrix of a cracked element with constraints may be calculated. The additional strain energy due to the crack results in a local flexibility matrix $[C_c]$, which has already been obtained above in section 3.1.

TABLE 1

Rotor–bearing data

Operating speed of rotor	60 rad/s
Torsional frequency	25 rad/s
Length of the rotor, L	50 cm
Shaft	
Diameter, D	2 cm
Density and elastic modulus	7800 kg/m^3, 2·08 E11 N/m^2
Disc	
Location	Mid-span
Mass, m	5·5 kg
Polar moment of inertia, I_P	0·01546 kg m^2
Diametral moment of inertia, I_D	0·00773 kg m^2
Unbalance eccentricity, e	0·1 mm
Crack location, Z/L	0·4
Bearing (isotropic)	
Stiffness	10^5 N/m
Damping	100 Ns/m

To obtain the total flexibility of the cracked element one must add the local flexibility due to the crack [11–13]. The total flexibility matrix for the cracked section is given as $[C] = [C_0] + [C_c]$.

Considering six degrees of freedom (d.o.f.) at each node—that is, 12 d.o.f. for the element and from the equilibrium condition (see Figure 3)—the following equation can be written:

$$(q_1, q_2, \ldots, q_{12})^{\mathrm{T}} = [T](q_7, \ldots, q_{12})^{\mathrm{T}}, \tag{7}$$

where the transformation matrix is

$$T = \begin{bmatrix} -1 & 0 & 0 & 0 & 0 & 0 \\ 0 & -1 & 0 & 0 & 0 & 0 \\ 0 & 0 & -1 & 0 & 0 & 0 \\ 0 & 0 & -l & -1 & 0 & 0 \\ 0 & l & 0 & 0 & -1 & 0 \\ 0 & 0 & 0 & 0 & 0 & -1 \\ 1 & 0 & 0 & 0 & 0 & 0 \\ 0 & 1 & 0 & 0 & 0 & 0 \\ 0 & 0 & 1 & 0 & 0 & 0 \\ 0 & 0 & 0 & 1 & 0 & 0 \\ 0 & 0 & 0 & 0 & 1 & 0 \\ 0 & 0 & 0 & 0 & 0 & 1 \end{bmatrix}.$$

Using the principle of virtual work, the stiffness matrix of the cracked element can be written as [12, 13]

$$[K_c] = [T][C]^{-1}[T]^{\mathrm{T}}. \tag{8}$$

TABLE 2

Eigenfrequencies of undamped and uncracked rotor–bearing system

Mode	Eigenfrequency (rad/s)
1	152·5
2	598·2
3	1733·6

4. THE SYSTEM EQUATION OF MOTION

Nelson and McVaugh [14] presented a finite element model using Rayleigh's beam theory for a rotor–bearing system consisting of rigid discs, distributed parameter finite shaft elements and discrete bearings. Ozguven and Ozkan [15] presented an extended model by synthesizing the previous models. The present study uses these models by including the slant crack model. In addition, the axial and torsional mode shape functions are derived by assuming a linear variation along the z-axis of the element [16]. No coupling between the axial, bending and torsional modes is assumed while deriving the matrices. The shaft is discretized into finite beam elements (Figure 3). As shown in Figure 3, each element has six degrees of freedom at each node, represented by q_1–q_{12} (although the element is shown with a slant crack, the degrees of freedom considered are the same for an uncracked element as well). The discrete bearing stiffness and damping and the rigid disc mass parameters are considered at the corresponding degrees of freedom, after assembling the different shaft elements.

Assembling the different rotor components, the equation of motion of the complete rotor system in a fixed co-ordinate system (see Figure 3), can be written as

$$[M]\{\ddot{q}\} + [D]\{\dot{q}\} + [K]\{q\} = \{Q\}, \tag{9}$$

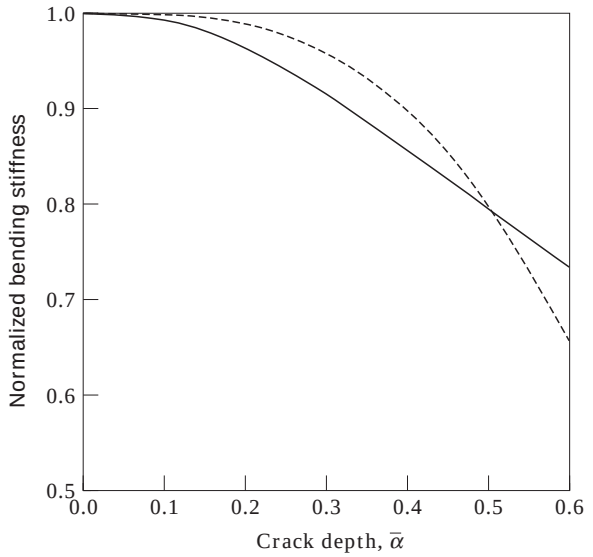

Figure 5. Variation of the normalized bending stiffness with the slant crack depth. ——, K_{XX}; – – – –, K_{YY}.

where the mass matrix includes the rotary and translational mass matrices of the shaft, the rigid disc mass and the diametral moments of inertia. The matrix D includes the gyroscopic moments and bearing damping. The stiffness matrix considers the stiffnesses of the shaft, the bearing and the cracked shaft element. The details of the individual matrices of equation (9), except for that of cracked shaft element, are given in references [14–16].

4.1. INCORPORATION OF CRACKED SHAFT

The details of the stiffness matrix of the slant cracked shaft element are discussed in section 3. The crack is assumed to affect only the stiffness. The element with a crack will

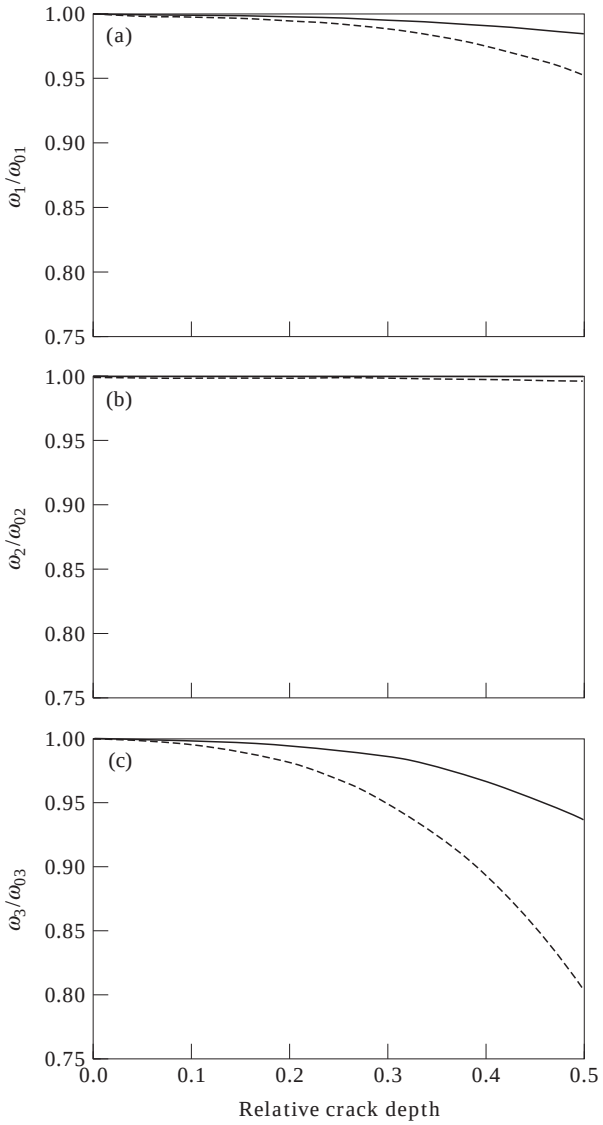

Figure 6. Variation of eigenfrequencies with the relative crack depth. ——, Slant crack; – – – –, transverse crack.

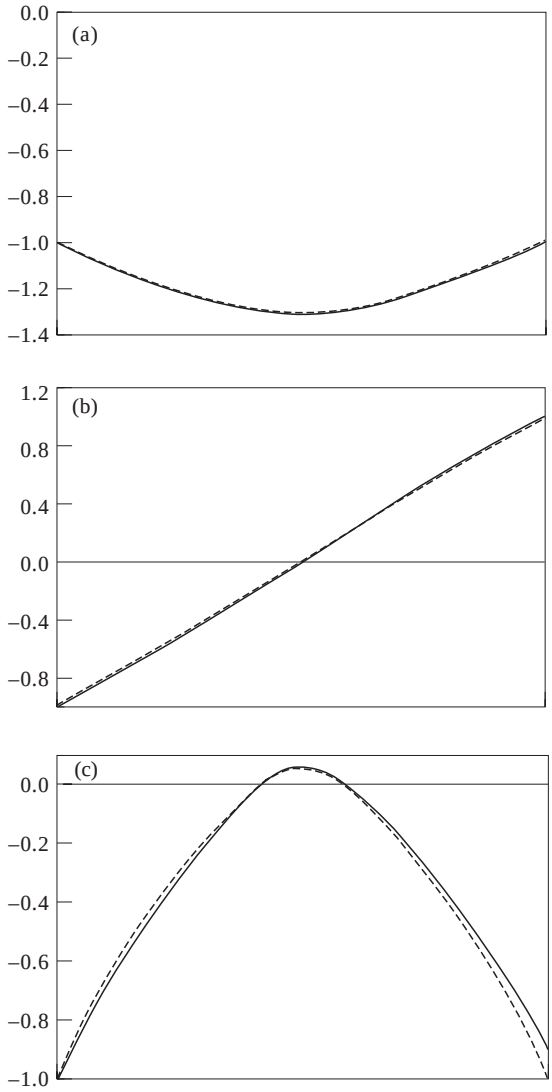

Figure 7. Variation of mode shapes with the slant crack depth. – – – –, No crack; ——, $\bar{\alpha} = 0{\cdot}5$.

replace the corresponding uncracked element while assembling different rotor components in equation (9) resulting in $[\bar{K}]$, the system stiffness matrix. For eigenvalue analysis, the crack is assumed to be open. The eigenfrequencies are obtained by solving the eigenvalue problem $[K] - \omega^2[M] = 0$, and $[\bar{K}] - \omega^2[M] = 0$, for the uncracked and cracked shafts, respectively. However, stiffness variation with time and torsional frequency for the cracked element is considered below for the steady state response, and this element will replace the uncracked element.

4.2. MODELLING OF BREATHING PHENOMENA

It has been mentioned in section 2 that the slant crack is generated because of torsional vibration, and opens and closes (i.e., ''breaths'') with torsional vibrations of the shaft. The moment of inertia of the section containing the crack will be higher when a negative

moment is applied. As the bending stiffness of the shaft is proportional to the inertia of the section of the shaft, we expect the bending stiffness of the shaft with slant crack to change synchronously with the torsional vibration.

The variation of the stiffness of the cracked element can be expressed by a truncated cosine series [17]:

$$[K] = [K(\omega_T t)] = [K_0] + [K_1]\cos(\omega_T t) + [K_2]\cos(\omega_T t) + [K_3]\cos(\omega_T t), \tag{10}$$

where $[K_n]$, $n = 0, \ldots, 3$ are the fitting coefficient matrices determined from the known behaviour of the stiffness matrices at certain angular locations, as given in reference [17]. For smooth transition from open to closed, one can consider the half crack condition as satisfied in references [17, 18]. However, only fully open or fully closed conditions of the

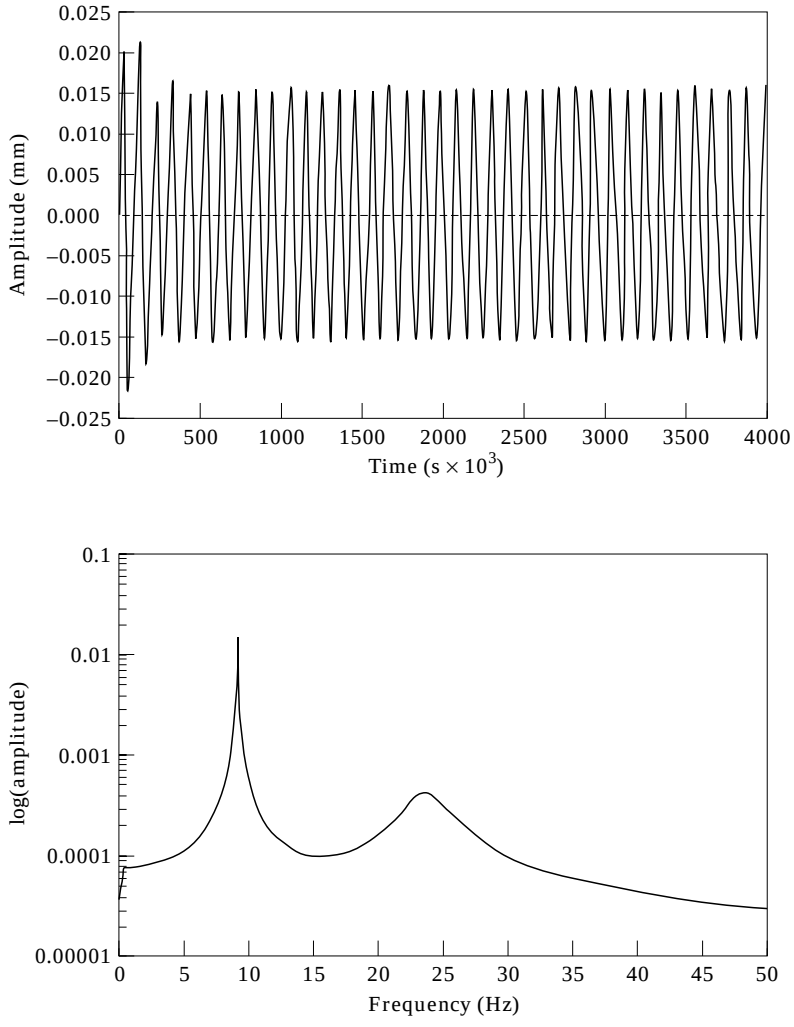

(a)

Figure 8(a).

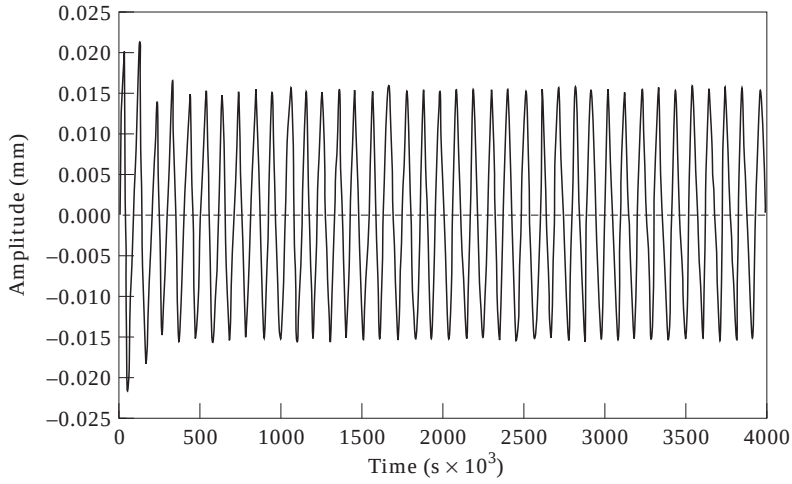

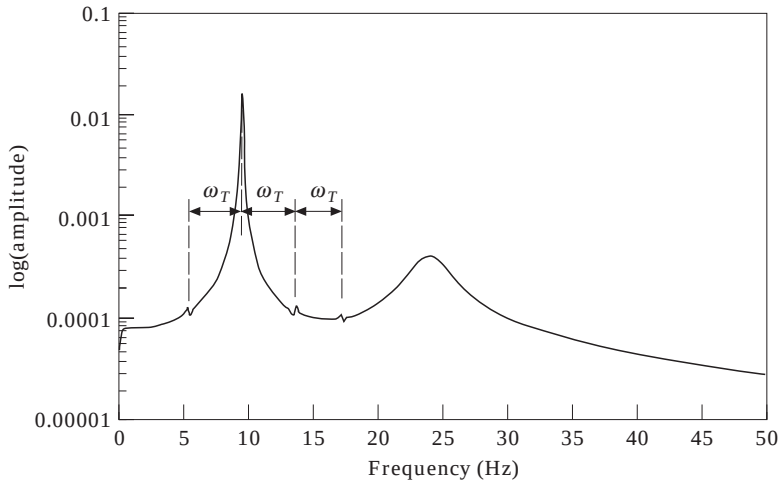

(b)

Figure 8.—*continued*.

crack are considered here. When the crack is fully closed, the shaft element will be treated as uncracked. The following conditions are used for the breathing:

$$\text{at } \omega_T t = 0,\ [K] = [K]_{UC} \qquad \text{and} \qquad \partial^2/\partial\phi^2[K] = 0,$$

$$\text{at } \omega_T t = \pi,\ [K] = [K]_{op} \qquad \text{and} \qquad \partial^2/\partial\phi^2[K] = 0,$$

where $\phi = \omega_T t$ and UC and op denote uncracked and open crack conditions, respectively.

With the above conditions, we evaluate

$$[K_0] = ([K]_{op} + [K]_{UC})/2, \qquad [K_1] = 9([K]_{UC} - [K]_{op})/16,$$

$$[K_2] = 0, \qquad [K_3] = ([K]_{op} - [K]_{UC})/16, \tag{11}$$

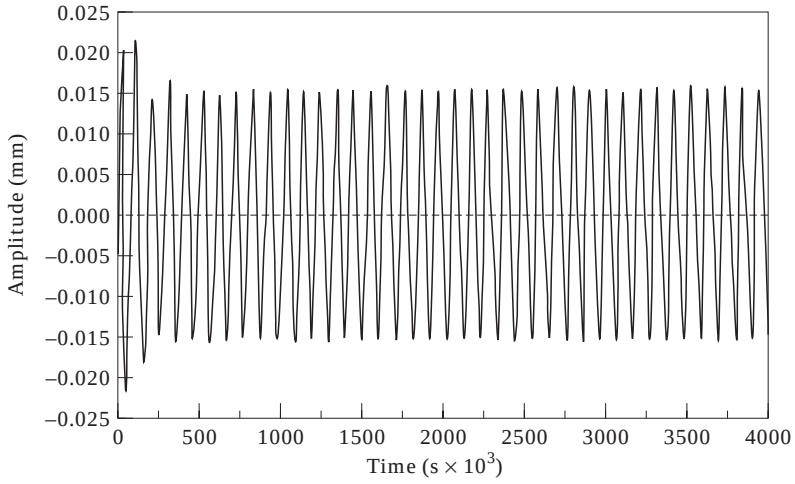

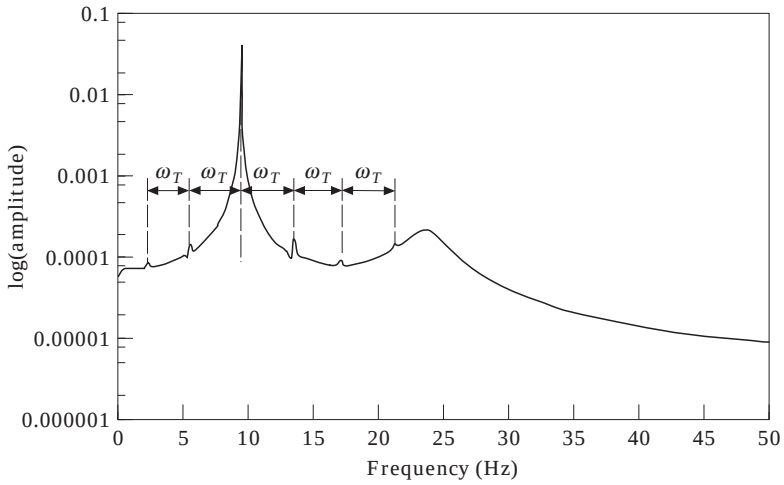

(c)

Figure 8.—*continued*.

where $[K]_{op}$ and $[K]_{UC}$ are for the open and uncracked conditions respectively. These can be obtained from the compliance matrices C_0 and C, and by using equation (8). Thus the stiffness of the cracked element at any time can be obtained if torsional frequency ω_T is known.

In the present study, the Houbolt time marching technique [18] has been used to model the system and obtain the steady state response in the time domain. Although the stiffness varies with time when the shaft is cracked, during a small time step, the stiffness was assumed to be constant and the same time marching scheme was used.

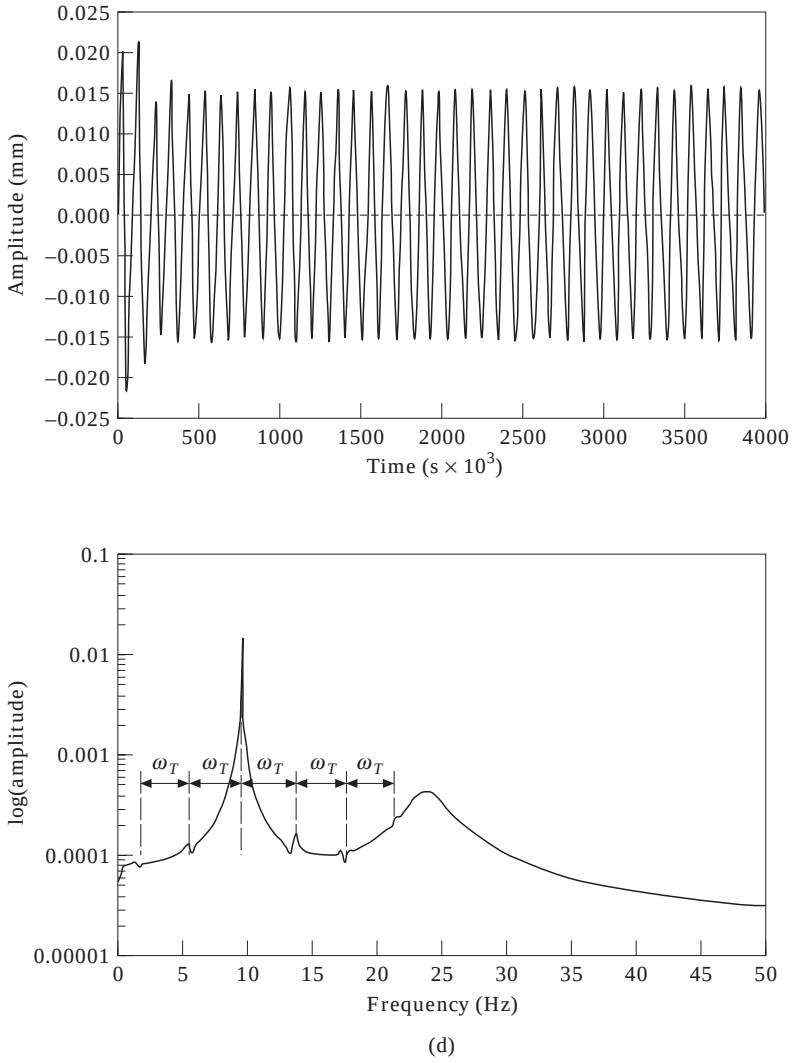

(d)

Figure 8(d)

Figure 8. The steady state responses and frequency spectra of the rotor. (a) No slant crack; (b) slant crack depth, $\bar{\alpha} = 0{\cdot}2$; (c) slant crack depth, $\bar{\alpha} = 0{\cdot}3$; (d) slant crack depth, $\bar{\alpha} = 0{\cdot}4$.

5. RESULTS AND DISCUSSION

The rotor shaft is discretized into 25 finite elements. The stiffness matrix of the cracked element replaces the uncracked element while assembling for the rotor–bearing system. The data used for the rotor–bearing system with slant crack are shown in Table 1. For the eigenfrequency analysis, the crack is considered as open. Simultaneous iteration techniques are used to solve the undamped eigenvalue problem. The eigenfrequencies for an undamped and uncracked rotor are given in Table 2. The bending stiffness of the cracked element is different in the X- and Y-directions, the variation with crack depth being clearly visible in Figure 5. Here, the normalization is carried out with that of the uncracked element.

The variation of eigenfrequencies in different modes of the rotor with slant and transverse [13] crack depths is shown in Figures 6(a–c). The comparison in Figures 6(a–c) shows that the eigenfrequencies decrease with slant crack depth in a similar way as in the case of a transverse crack [13]. This is expected, as the slant crack also reduces the effective stiffness of the rotor system. However, the decrease in eigenfrequencies depends on how close the crack is to the node of the corresponding mode shape. This can be clearly seen by observing the mode shapes shown in Figures 7(a–c). It is also found from Figures 6(a–c) that the decrease in eigenfrequencies is smaller with relative crack depth, for the same crack location (Z/L), in the case of the slant crack being compared to that of the transverse crack. However, the detection of the slant crack can be done effectively by considering the steady state and transient responses.

The steady state responses of the rotor and corresponding frequency spectra (obtained from the fast Fourier transform (FFT)) are shown in Figures 8(a–d) for different crack depths. Since the running speed of the rotor is 60 rad/s (9·54 Hz), there is a synchronous frequency at 9·54 Hz in the spectra. When the crack depth increases, however, it can be noticed that the subharmonic frequencies are centered on 9·54 Hz in Figures 8(b–d). The interval frequency of this subharmonic vibration is equal to 3·97 Hz, which is the same as the torsional frequency (25 rad/s) of the rotor. These results match well with the findings in references [9, 10].

It was shown in reference [9] that the steady state response of the rotor system with a slant crack on its shaft induced by unbalance contains frequencies represented by $\omega_n = \Omega \pm n\omega_T/2$; $m = 1, 2, \ldots$ and $n = 0, 1, 2, \ldots$, where Ω is the operating speed of the rotor and ω_T is the frequency of torsional vibration of the rotor system. However, in the present numerical results, observations similar to those in reference [9] are made where only terms that are even in n are satisfied (see Figures 8(a–d)). The frequencies are represented by $\omega_n = \Omega \pm n\omega_T$.

The results of the present study agree well with those of reference [9]. The aim of the present study is to develop a stiffness matrix of the slant cracked element so as to use it easily in FEM analysis. This work can easily be extended to further studies such as transient and stability analysis.

6. CONCLUSIONS

In the present study an FEM analysis of a rotor–bearing system for flexural vibrations has been considered by including a shaft having a slant crack.

A flexibility matrix for the slant crack has been derived, on similar lines as in the work of Papadopoulos and Dimarogonas [11] for a transverse crack. This is used to develop the stiffness matrix of a slant cracked element, for subsequent use in FEM analysis of the rotor–bearing system.

A general trend of a reduction in the eigenfrequencies of all of the modes with an increase in crack depth has been observed. This behaviour is similar to the case of the transverse crack. However, it is observed that the decrease in eigenfrequencies with relative crack depth, for the same crack location, is smaller in the case of a slant crack compared to that of a transverse crack.

The frequency spectrum of the steady state response of the cracked rotor was found to have subharmonic frequency components at an interval frequency corresponding to the torsional frequency, which can be used for crack detection.

This work can easily be extended to further studies such as transient and stability analysis.

REFERENCES

1. A. D. Dimarogonas 1970 *Dynamic Response of Cracked Rotors*. Technical Information Series. Schenectady, New York: General Electric Co.
2. T. Pafelias 1974 *No. DF-74-LS-79*. Dynamic behavior of a cracked rotor. Technical Information Series. Schenectady, New York: General Electric Co.
3. P. G. Kirmser 1944 *Proceedings of the ASTM* **44**, 897–904. The effect of discontinuities on the natural frequency of beams.
4. W. J. Thomson 1949 *Journal of Applied Mechanics* **17**, 203–207. Vibration of Slender bars with discontinuities in stiffness.
5. A. D. Dimarogonas and S. A. Paipetis 1983 *Analytical Methods in Rotor Dynamics*. London: Applied Science Publishers. See pp. 144–193.
6. J. Wauer 1990 *Applied Mechanics Reviews* **43**, 13–17. Dynamics of cracked rotors: literature survey.
7. R. Gasch 1993 *Journal of Sound and Vibration* **160**, 313–332. A survey of the dynamic behaviour of a simple rotating shaft with a transverse crack.
8. A. D. Dimarogonas 1996 *Engineering Fracture Mechanics* **55**, 831–857. Vibration of cracked structures: a state of the art review.
9. M. Ichimonji and S. Watanabe 1988 *Japan Society of Mechanical Engineers*, *International Journal*, *Series III* **31**(4), 712–718. The dynamics of a rotor system with a shaft having a slant crack (a qualitative analysis using a simple rotor model).
10. M. Ichimonji, Y. Kazao, S. Watanabe, and S. Nonaka 1994 *Nonlinear and Stochastic Dynamics*, *ASME*, *AMD*-192/*DE*-78, *International Mechanical Engineering Congress and Exposition*, *Chicago*, *Illinois*, 81–90. The dynamics of a rotor system with a slant crack under torsional vibration.
11. C. A. Papadopoulos and A. D. Dimarogonas 1987 *Journal of Sound and Vibration* **117**, 81–93. Coupled longitudinal and bending vibrations of a rotating shaft with an open crack.
12. G.-L. Qian, S. N. Gu and J.-S. Jiang 1990 *Journal of Sound and Vibration* **138**, 233–243, The dynamic behaviour and crack detection of a beam with a crack.
13. A. S. Sekhar and B. S. Prabhu 1994 *Journal of Sound and Vibration* **169**, 655–667. Vibration and stress fluctuations in cracked shafts.
14. H. D. Nelson and J. M. McVaugh 1976 *Transactions of the American Society of Mechanical Engineers*, *Journal of Engineering for Industry* **98**(2), 593–600. The dynamics of rotor–bearing systems using finite elements.
15. H. N. Ozguven and Z. L. Ozkan 1984 *Transactions of the American Society of Mechanical Engineers*, *Journal of Vibration*, *Acoustics*, *Stress and Reliability in Design* **106**, 72–79. Whirl speeds and unbalance response of multi-bearing rotor using finite elements.
16. S. S. Rao 1980 *The Finite Element Method in Engineering*. Oxford: Pergamon Press.
17. C. A. Papadopoulos and A. D. Dimarogonas 1988 *Transactions of the American Society of Mechanical Engineers*, *Journal of Vibration*, *Acoustics*, *Stress and Reliability in Design* **110**, 356–359. Stability of cracked rotors in the coupled vibration mode.
18. A. S. Sekhar and B. S. Prabhu 1994 *Journal of Sound and Vibration* **173**, 415–421. Transient analysis of a cracked rotor passing through critical speed.

APPENDIX: NOMENCLATURE

$[C]$ flexibility matrix with crack
$[D]$ matrix includes gyroscopic effects and damping
D diameter of shaft
e unbalance eccentricity of the rotor
E modulus of elasticity
I_D diametral moment of inertia
I_P polar moment of inertia
$[K]$ stiffness matrix
l element length
L length of rotor
$[M]$ mass matrix
M_Z torsional moment
$\{q\}$ vector for nodal quantities

$\{Q\}$ force vector
t time
Z location of crack
α crack depth
$\tilde{\alpha}$ $= \alpha/D$
ω_{0i} eigenfrequency of uncracked rotor for ith mode
ω_i eigenfrequency of cracked rotor for ith mode
ω_T torsional frequency